Available online at www.sciencedirect.com

SCIENCE DIRECT®

Remote Sensing of Environment 95 (2005) 231–247

Remote Sensing of Environment

www.elsevier.com/locate/rse

# Effects of channel morphology and sensor spatial resolution on image-derived depth estimates

Carl J. Legleiter[a,b,*], Dar A. Roberts[a]

[a]Geography Department, University of California Santa Barbara, Ellison Hall 3611, Santa Barbara, CA 93106, United States
[b]Yellowstone Ecological Research Center, Bozeman, MT 59715, United States

Received 18 August 2004; received in revised form 20 December 2004; accepted 24 December 2004

**Abstract**

The utility of remote sensing in the study of fluvial systems depends upon the extent to which image data can be used to derive quantitative information of sufficient accuracy and precision for specific applications. In this study, we evaluate the effects of channel morphology on depth retrieval by coupling a radiative transfer model to various morphologic scenarios. Upwelling radiance $L_u$ spectra generated for a range of depths (2–150 cm) and benthic cover types (limestone, periphyton, and gravel) were linearly mixed to simulate sub-pixel bed topography and substrate heterogeneity. For sloping bottoms, solar–streambed geometry modified $L_u$ relative to a level bottom, especially for beds sloping steeply away from the sun. Aggregate pixel scale $L_u$ spectra were compared to a database of simulated spectra to determine the radiance-equivalent depth of a uniform bottom (*REDUB*). *REDUB* spectra for hypothetical stepped streambeds indicated underestimation of the actual area-weighted mean depth, but the ln ($L_{u,560}/L_{u,690}$) *REDUB* ratio consistently reproduced the pixel-scale mean for beta distributions of depths. Similarly, when both dark periphyton and bright limestone substrates occurred within a pixel, *REDUB* spectra produced large errors while the ratio proved robust. Along channel banks, pixels will inevitably be mixed, and our simulations indicated that although bank fractions estimated by spectral mixture analysis were highly accurate for vegetated cutbanks, gravel bars were sensitive to the selection of both aquatic and terrestrial end members and subject to relatively large fraction errors. These theoretical results were tested using a ratio-based relative depth map and two-end member mixture models derived from a hyperspectral image of the Lamar River in Yellowstone National Park, which also served to illustrate the importance and applicability of our simulations. The primary conclusions of this study are that 1) the ratio-based algorithm is well-suited to complex river channels; 2) channel morphology and sensor spatial resolution must be considered jointly during data collection and analysis; and 3) the accuracy and precision of depth estimates are influenced by channel morphology and thus vary spatially.


*Keywords:* River channel; Remote sensing; Depth; Radiative transfer model; Spectral mixture analysis; In-stream habitat

## 1. Introduction

Remote sensing has emerged as a potentially powerful tool for detailed, quantitative characterization of fluvial systems across broad geographic areas with improved temporal coverage (Mertes, 2002). Since the early 1990's, numerous studies have demonstrated the utility of remotely sensed data for retrieving suspended sediment concentrations (Mertes et al., 1993), classifying in-stream habitat (Legleiter & Goodchild, 2005; Whited et al., 2002; Wright et al., 2000), and estimating water depth (Lyon et al., 1992; Marcus et al., 2003; Winterbottom & Gilvear, 1997). When multi-temporal image data are available, the synoptic perspective offered by aerial platforms has allowed geomorphologists to document channel changes associated with flood events (Bryant & Gilvear, 1999) and estimate volumes of erosion and deposition in large, braided river systems (Lane et al., 2003). Recent increases in the number and

* Corresponding author. Geography Department, University of California Santa Barbara, Ellison Hall 3611, Santa Barbara, CA 93106, United States.
*E-mail addresses:* carl@geog.ucsb.edu (C.J. Legleiter), dar@geog.ucsb.edu (D.A. Roberts).

0034-4257/$ - see front matter © 2005 Elsevier Inc. All rights reserved.
doi:10.1016/j.rse.2004.12.013

diversity of remote sensing systems, including high spatial resolution commercial satellites, imply that spectrally-driven, image-based analyses could become an integral component of river research and management.

Ultimately, however, the utility of remote sensing technology will depend on the degree to which the channel characteristics of interest can be remotely measured with the accuracy and precision required for specific applications. Although most previous stream research has been empirical, relating image-derived quantities to ground-based measurements (Marcus et al., 2003; Winterbottom & Gilvear, 1997), a more thorough knowledge of the underlying physical principles is needed to quantify uncertainties and define realistic operational guidelines. As a first step toward a general theoretical framework, Legleiter et al. (2004) used a radiative transfer model to illustrate the effects of water depth, substrate reflectance, suspended sediment, and surface turbulence on the upwelling spectral radiance from a shallow stream channel. We concluded that, although certain fundamental limitations must be acknowledged, remote mapping of river channel morphology and in-stream habitat is both theoretically sound and technically feasible. In particular, our radiative transfer simulations and ground-based spectral measurements demonstrated that a simple ratio-based algorithm could provide an image-derived quantity linearly related ($R^2$=0.79) to water depth across a range of stream conditions.

Our initial work described radiative transfer processes and discussed the role of sensor spectral and radiometric resolution but did not specifically address the spatial effects that could prove to be a limiting factor in small-to moderate-sized channels (Legleiter et al., 2002; Wright et al., 2000). In these highly variable, dynamic systems, biotic and geomorphic patterns and interactions often occur at a spatial scale finer than the spatial resolution of the imaging system, typically equated with the pixel edge dimension (but see Cracknell, 1998). Such incongruence between the scales at which data are collected and processes operate represents a classic problem in remote sensing and geographic information science that has also drawn attention in the marine research community (e.g., Andrefouet et al., 2002). Recent emphasis on shallow coastal environments, primarily coral reefs (e.g., Andrefouet et al., 2003), has motivated studies on the effects of bottom morphology and fine-scale substrate variability (Mobley & Sundman, 2003; Zaneveld & Boss, 2003).

In this paper, we draw upon coastal research to evaluate a fundamental question: can remotely sensed data be used to effectively document the subtle channel changes of interest to the fluvial geomorphologist? For applications such as post-project appraisal of river restoration projects (Downs & Kondolf, 2002) and morphologic estimation of sediment transport rates (Ashmore & Church, 1998; Gaeuman et al., 2003), accurate characterization of channel bed topography is critical (Lane, 1998). The use of raster-formatted image data in these studies entails two basic limitations: 1) even when depth varies on a sub-pixel scale, only one depth estimate can be assigned to each image pixel; and 2) along channel banks, radiance is contributed from both terrestrial and aquatic features and pixels will inevitably be mixed. The former problem is expected to complicate depth retrieval to a degree dependent upon the complexity of channel bed topography and benthic cover and the dimensions of an image pixel, whereas the latter problem could influence measurements of channel width and preclude near-bank depth estimates. Our goal in this paper is to evaluate the effects of channel morphology and sensor spatial resolution on image-derived depth estimates. Specifically, we use tools developed by oceanographic and terrestrial remote sensing scientists—radiative transfer modeling and spectral mixture analysis, respectively—to address a pair of basic questions:

1) When depth or substrate reflectance varies within an image pixel, what is the composite upwelling spectral radiance signal recorded by a remote sensing system? What will be the resulting, single depth estimate for that pixel?
2) What are the spectral characteristics of mixed pixels along channel banks? Can these pixels be unmixed to refine estimates of channel width?

## 2. Methods

### 2.1. Field data collection and archival image data

The Lamar River basin of northeastern Yellowstone National Park, USA, has been the subject of several previous remote sensing studies (e.g., Marcus et al., 2003; Wright et al., 2000) and ongoing research on channel change. The field data for this study were acquired along Soda Butte Creek, a major tributary of the Lamar River, in July and August, 2003, and consist of point measurements of water depth and a spectral library of channel substrates and bank cover types (Fig. 1, Table 1). The collection and processing of the spectral data are described in Legleiter et al. (2004). Water depths in Soda Butte Creek averaged 38 cm, with a slightly positively skewed distribution and a maximum of 142 cm; the Lamar River is slightly deeper on average, with a maximum measured depth of 160 cm (Marcus et al., 2003). The substrate in these streams consisted primarily of gravel derived from glacial outwash, andesitic volcanic rocks, and Paleozoic carbonates (Prostka et al., 1975); a few reaches of Soda Butte Creek flow over limestone bedrock. As flows subside in mid- to late summer, periphyton coats portions of the streambed as well, typically in shallow, low-velocity areas.

Hyperspectral image data for the Lamar River were acquired by the AISA sensor on August 1, 2002. This instrument recorded upwelling spectral radiance in 34 narrow bands (full-width half-maximum of 3.10–3.42 nm)

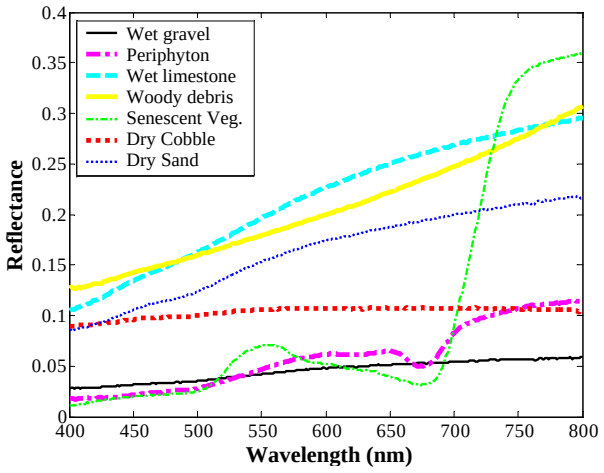


Fig. 1. Reflectance spectra for substrate types and stream bank materials from the spectral library compiled along Soda Butte Creek in Yellowstone National Park (Legleiter et al., 2004).

spanning the visible/near-infrared spectral region from 495–898 nm. Apparent at-platform reflectance was calculated from concurrent measurements of downwelling spectral irradiance, obtained using a diffuse collector mounted on top of the aircraft and connected to the AISA sensor by a fiber optic cable (http://www.specim.fi/products-aisa.html). The ground sampling distance of 2.5 m produced many mixed pixels along the banks of the 30–50 m wide channel and dictated that most in-stream pixels would encompass a range of depths and/or substrate types. Although ground reference data for this time period were not available, we intend to use the AISA image as part of a time series for monitoring channel change in northern Yellowstone. Here, we present a scene from the Lamar River to evaluate the results of the radiative transfer simulations that are the primary focus of this paper and to illustrate the real-world applicability of these modeled scenarios.

### 2.2. Radiative transfer modeling

In essence, passive optical remote sensing of fluvial systems is based upon spatially distributed measurements of a fundamental physical quantity, the upwelling spectral radiance. For a shallow stream channel, this reflected solar energy can be conceptualized as the sum of five components:

$$L_T = L_P + L_S + L_C + L_B + L_L, \quad (1)$$

where $L_T$ is the total at-sensor spectral radiance; $L_P$ represents path radiance scattered into the sensor's field of view by the Earth's atmosphere; $L_S$ denotes radiance reflected from the water surface, interacting with neither the water column nor the substrate; $L_C$ refers to radiance that entered the water column but was scattered into the upper hemisphere before reaching the bottom; $L_B$ is the portion of $L_T$ that reflected from the streambed, passed through the air–water interface, and traveled through the atmosphere to the sensor; and $L_L$ is the radiance contribution from adjacent areas of land, typically gravel bars or riparian vegetation, for mixed pixels along the channel banks. Of these components, only the last is directly relevant to characterization of channel morphology (i.e., water depth) and in-stream habitat (i.e., benthic cover). Our analysis thus focused upon the two primary controls on $L_B$, bottom depth $z_b$ and the (spectral irradiance) reflectance of the substrate $R_\lambda$, by using a radiative transfer model to simulate $L_T$ spectra while fixing the parameters that determine $L_P$, $L_S$, $L_C$, and $L_L$.

The radiative transfer equation describes the attenuation of electromagnetic radiation within the water column and can be solved numerically, subject to certain critical assumptions, if initial and boundary conditions are specified (Mobley, 1994). The Hydrolight computer model (Mobley & Sundman, 2001) implements these solution methods to simulate spectral radiance distributions within and above a water column and is used extensively in various marine environments (e.g., Dierssen et al., 2003; Louchard et al., 2003). Individual Hydrolight runs are parameterized by $z_b$ and $R_\lambda$, as well as water column optical properties, water surface state, solar geometry, and atmospheric conditions. This one-dimensional model assumes that all changes in the underwater light field are functions of depth alone, independent of horizontal location; this simplified geometry

Table 1
Input parameters for the Hydrolight radiative transfer model

| Parameter type | Value or range of inputs | Description |
|---|---|---|
| Solar geometry | 20°, 30°, 40°, 50°, 60° | Solar zenith angle in air |
| Sea level pressure | 1016 mbar | |
| Air mass type | 10 | Continental |
| Relative humidity | 20% | |
| Precipitable water | 0.5 cm | |
| 24-hr average wind speed | 0 m/s | |
| Horizontal visibility | 100 km | |
| Water depth | 2–150 cm in steps of 1 cm | |
| Substrate reflectance (ground-based spectral measurements) | Periphyton | Samples scraped from cobbles removed from streambed |
| | Wet gravel | Mixture of rock types and particle sizes, measured on gravel bars |
| | Wet limestone | Mississippian Madison Limestone Group (Prostka et al., 1975); Grey-white (Munsell color chart: Hue 0.19Y, Value 5.71, Chroma 2.87) |
| Suspended sediment concentration | 2 g/m$^3$ | Converted to inherent optical properties using brown earth optical cross-section |
| Wind speed | 5 m/s | Surrogate for flow turbulence |

allows for numerical solution of the radiative transfer equation. For more complex, three-dimensional configurations where bottom depth and/or albedo vary spatially (i.e., river channels), computationally expensive probabilistic methods are technically more appropriate. Mobley and Sundman (2003), however, found close agreement between Hydrolight and a backward Monte Carlo model (BMC3D) in the presence of fine-scale substrate variability (errors<1%) and sloping bottoms (errors<7% for bottom slopes<20°), concluding that efficient one-dimensional models can predict radiance distributions above heterogeneous bottoms with sufficient accuracy for all but the most demanding applications. For our first-order analysis, we therefore adopt this plane-parallel approximation and use the Hydrolight radiative transfer model to simulate the effects of sub-pixel variability of depth and bottom albedo.

We developed a database of 2,235 simulated Hydrolight spectra parameterized by the input data in Table 1. The incident spectral irradiance $E_d$ and sky radiance distribution for our study area in Yellowstone National Park were obtained using the Gregg and Carder (1990) and Harrison and Coombes (1988) models, respectively; cloud cover was assumed negligible. To isolate the effects of depth and bottom albedo, suspended sediment concentration was fixed at 2 g/m$^3$ and the brown earth optical cross-section included with Hydrolight used to obtain the corresponding absorption ($a$) and scattering ($b$) coefficients (Bukata et al., 1995). The concentration profile was vertically homogeneous and the contributions of chlorophyll and dissolved organic matter to the inherent optical properties of the water column were assumed negligible. In practice, the abundance and wavelength-dependent scattering and absorption properties of various constituents suspended and/or dissolved within the flow will also influence $L_u$ and thus depth retrieval and substrate characterization. Surface turbulence was incorporated by fixing the wind speed, which Hydrolight uses to generate an irregular water surface described by the Cox and Munk (1954) wave slope statistics (Mobley, 1994), at 5 m/s. Substrate $R_\lambda$ spectra for three bottom types were used, including bright white-gray limestone, periphyton scraped from streambed cobbles, and gravel of mixed grain size and lithology (Fig. 1, Table 1). For each substrate type, simulated spectra were generated for bottom depths ranging from 2 to 150 cm in 1 cm increments. Shallower and/or more closely spaced depths could not be modeled because Hydrolight computes diffuse attenuation coefficients (e.g., $K_d$, defined as the depth derivative of the downwelling plane irradiance $E_d$; Mobley, 1994) using a finite difference approximation that dictates a minimum spacing between successive output depths. All depths shallower than 2 cm in our simulations were therefore assigned the corresponding $L_u$ spectra for a depth of 2 cm. To evaluate the effect of solar geometry, a separate set of Hydrolight runs for all depth/substrate combinations was performed for in-air solar zenith angles $\theta_s$ from 20° to 60°, in 10° increments. The modeled spectra spanned the range 400–800 nm as a series of 100 monochromatic runs spaced 4 nm apart.

### 2.3. Simulated spectral mixtures

We examined the effects of sub-pixel variation of depth and bottom albedo and mixed stream bank pixels by simulating spectral mixtures, with an assumption of linear mixing. Under this framework, the composite spectral radiance $L_\lambda$ from a pixel containing multiple cover types (or bottom depths) is the sum of the $L_\lambda$ for each cover type, weighted by their areal abundance—that is, the spectral proportions match the spatial proportions (Adams et al., 1993). The use of additive mixtures neglects the contribution of multiply scattered photons to the total radiance, and our simulated mixtures therefore do not account for in-water adjacency effects. In shallow stream channels, however, these effects are likely to be minimal because the scattering phase function is strongly forward-peaked and depths are typically only one or two photon mean free paths $1/c$, where $c=a+b$ is the beam attenuation coefficient (Mobley & Sundman, 2003). Mobley and Sundman (2003, p.333) argued that under these circumstances, the vast majority of photons travel directly from the bottom to the water surface and the path radiance contribution is negligible, implying that scattering by the water column itself can be ignored. The validity of this assumption will be strained in deeper water and/or for higher suspended sediment concentrations, but provides a reasonable approximation for the shallow, clear water conditions in our study area.

Using the database of simulated Hydrolight spectra, we assembled fine-scale radiance fields by assigning the appropriate upwelling radiance $L_u$ (in air, just above the water surface) spectrum to each cell of various morphologic scenarios. Mixed pixels were then simulated by computing the average of the $L_u$ values for all 1 cm$^2$ cells encompassed by a pixel of the specified dimensions. We assumed square pixels and equally weighted the radiance contributions of all cells within the pixel; a more sophisticated radiance aggregation scheme could be used to model the point spread function of a particular sensor. For the stream bank scenarios, mixtures were modeled by combining the field-measured $R_\lambda$ spectra for the bank material types with $R_\lambda$ spectra for the submerged portion of the pixel, obtained from the Hydrolight-modeled $L_u$ by converting to irradiance (assuming isotropy and multiplying by $\pi$) and dividing by $E_d$.

### 2.4. Morphologic scenarios

Simulated spectra from the Hydrolight database were coupled to various bed configurations to model the effects of solar–streambed geometry, fine-scale morphology, and substrate heterogeneity on the pixel-scale upwelling spectral radiance that would be measured by a remote sensing system. Each scenario consisted of regular grids of depth

and substrate type with a cell size of 1 cm$^2$, and spectral properties were assigned from a look-up table. These scenarios are described in the following paragraphs and illustrated in Fig. 2.

To evaluate the effect of solar geometry and streambed slope and aspect, we considered a planar streambed rotated about both the vertical and horizontal axes. The bed sloped down at a specified angle $\theta_b$ and aspect $\varphi$ was defined as the angular difference between the slope direction and solar azimuth (Fig. 2a). Mobley and Sundman (2003) reasoned that the primary effect of a sloping bottom was to change the solar incidence angle and that the slope could be accounted for by using Lambert's cosine law to correct the radiance computed for a level bottom (i.e., with Hydrolight). We used

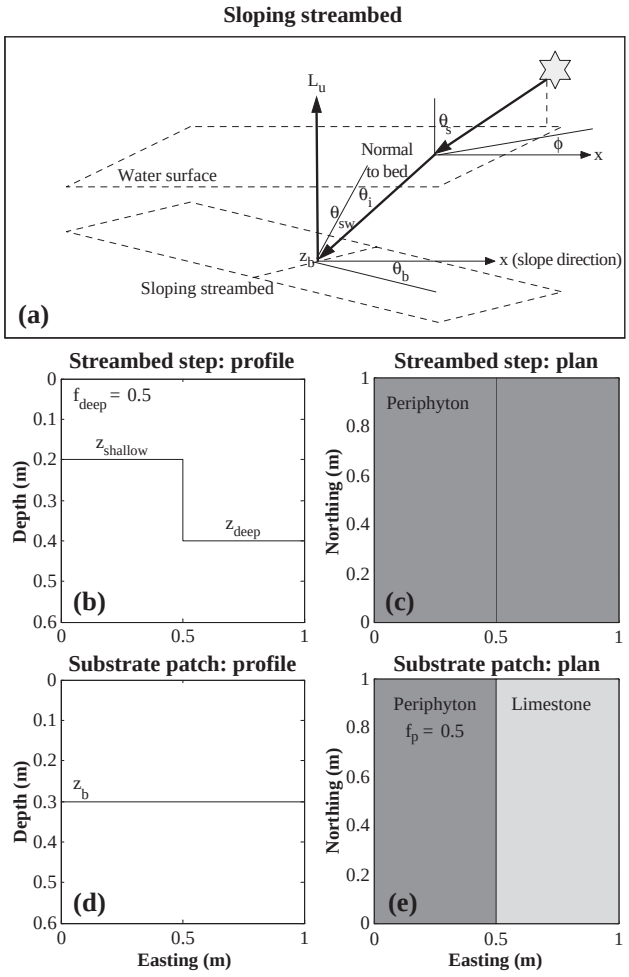


Fig. 2. Basic morphologic scenarios evaluated in this study. (a) A planar, sloping bed for modeling the effects of solar–streambed geometry. The bed slopes down in the $x$ direction at an angle of $\theta_b$ with the horizontal, the depth at which the upwelling spectral radiance $L_u$ is modeled as $z_b$, the solar zenith angle is $\theta_s$ in air and $\theta_{sw}$ in water, the solar azimuth (angular difference between the slope direction and the position of the sun) is $\varphi$, and the incidence angle of the solar beam onto the streambed is $\theta_i$, measured relative to the streambed normal. Profile (b) and plan (c) of a stepped streambed with a uniform substrate. Profile (d) and plan (e) of a heterogeneous substrate with a constant depth $z_b$. Scenarios evaluated for hypothetical 1 m$^2$ pixels. Figure after Mobley and Sundman (2003).

Eqs. (9) and (10) of Mobley and Sundman (2003) to compute the radiance from a sloping streambed as

$$L_u^{slope} = L_u^{level} \frac{\cos\theta_i^{slope}}{\cos\theta_i^{level}}, \quad (2)$$

where $\theta_i$ denotes the solar incidence angle onto the streambed and the superscripts refer to sloping and level bed configurations. For a sloping bed, $\theta_i$ is given by

$$\cos\theta_i^{slope} = \sin\theta_b \sin\theta_{sw} \cos\varphi + \cos\theta_b \cos\theta_{sw}, \quad (3)$$

where $\theta_{sw}$ is the solar zenith angle after refraction at the air–water interface.

The effects of sub-pixel depth variability were modeled by aggregating fine-scale radiance fields corresponding to a stepped streambed. A fraction $f_{deep}$ of the simulated pixel was assigned a relatively large depth $z_{deep}$ while the remaining 1-$f_{deep}$ was assigned a shallower depth $z_{shallow}$ (Fig. 2b). By varying these three parameters, we modeled composite, pixel-scale $L_u$ spectra for pixels ranging from predominantly deep to mostly shallow, with various step heights (i.e., intra-pixel depth differences); both sides of the step had the same substrate $R_\lambda$ and $\theta_s$ was fixed at 30°. To determine the effect of such sub-pixel morphologic features on depth retrieval, we compared the composite radiance from the stepped streambed to the $L_u$ spectra tabulated in the Hydrolight database by defining the radiance-equivalent depth of a uniform bottom (*REDUB*) for each wavelength as the depth at which $L_u$ from a flat bed is closest in absolute value to the composite radiance from a more topographically complex streambed.

More complex bed configurations were simulated as random variables drawn from a beta distribution defined by parameters $\alpha$ and $\beta$ and bounded by a specified minimum $z_{min}$ and maximum $z_{max}$ depth

$$f(z_b;\alpha,\beta,z_{min},z_{max}) = \frac{1}{z_{max}-z_{min}} \cdot \frac{\Gamma(\alpha+\beta)}{\Gamma(\alpha)\Gamma(\beta)} \times \left(\frac{z_b - z_{min}}{z_{max}-z_{min}}\right)^{\alpha-1} \times \left(\frac{z_{max}-z_b}{z_{max}-z_{min}}\right)^{\beta-1}, \quad (4)$$

where $f(\cdot)$ is the probability density function (pdf) of depths for $z_{min} \le z_b \le z_{max}$ (the beta distribution has zero density outside this interval), and $\Gamma(\cdot)$ is the gamma function (Devore, 2000). A single substrate reflectance was used for all 1 cm$^2$ cells and $\theta_s$ was fixed at 30°. The flexibility of the beta pdf allowed us to generate depth histograms skewed toward deep or shallow water, uniformly distributed across the specified range of depths, or centered about a single mean depth. To examine the effects of differing degrees of sub-pixel scale topographic complexity on depth retrieval, we used the log-transformed band ratio algorithm shown to provide an image-derived quantity linearly related to water depth (Legleiter et al., 2004), computing ln ($L_{u,560}/L_{u,690}$)

for both aggregate, pixel-scale radiances for the simulated streambeds and for individual $L_u$ spectra in the Hydrolight database. Analogous to the *REDUB* above, we define the *REDUB* ratio as the depth at which the log-transformed band ratio value computed for a level bottom is closest in absolute value to the ratio computed for the mixed, variable depth pixel.

Similar to the bed step scenario, we modeled the effects of sub-pixel substrate heterogeneity by assigning a specified fraction of a pixel to one substrate and the remainder to a second benthic cover type (Fig. 2c). For these simulations, bottom depth was held constant and $\theta_s$ was fixed at 30°. Because $L_u$ is a function not only of depth but also bottom albedo (Legleiter et al., 2004), fine-scale substrate heterogeneity might interfere with depth retrieval. To examine this possibility, we computed both wavelength-specific *REDUB* values and ln ($L_{u,560}/L_{u,690}$) *REDUB* ratio values for simulated constant depth/mixed substrate pixels.

### 2.5. Stream bank spectral mixture analysis

Along the margins of the channel, radiance is contributed from both the submerged streambed and adjacent exposed areas with various cover types. In this study, we considered two common stream bank configurations which often occur in tandem on the inner and outer banks of a meander bend, respectively: a gently sloping gravel bar and a steep, vegetated cutbank (Fig. 3). We modeled mixed pixels along the gravel bar by specifying the fraction of the pixel $f_b$ occupied by exposed gravel and the bed slope $\theta_b$ off the bar into the channel, retrieving the appropriate Hydrolight spectrum for each depth (depths shallower than 2 cm were assigned the spectrum for 2 cm depth; see Section 2.2) along the slope (1 $cm^2$ cell size), applying the slope correction (Eq. (2); $\theta_s$ fixed at 30° and $\varphi$ at 45°), converting the $L_u$ spectra to reflectance (Section 2.3), and adding the area-weighted reflectances of the submerged and exposed portions of the pixel. For the vegetated cutbank, pixel-scale mixtures were generated by specifying $f_b$ and the bottom depth $z_b$. The transition from bank top to channel bed was assumed to occur over a fixed distance of 10 cm, and the radiance from this zone was incorporated by computing the depths along the slope and applying the slope correction as for the gravel bar. The pixel-scale reflectance was obtained by summing the area-weighted contributions from the vegetated bank, the bank-to-bed submerged slope, and the flat streambed.

To determine the extent to which stream bank pixels can be unmixed on the basis of their spectral characteristics, we used spectral mixture analysis (SMA, Adams et al., 1993), a popular technique with numerous terrestrial applications that has recently been extended to shallow marine environments (Hedley & Mumby, 2003; Hedley et al., 2004), to estimate $f_b$ for different bank scenarios. The essence of SMA is to model the reflectance (or radiance) spectrum of a mixed pixel as a weighted linear combination of the spectra of two or more pure cover types, called end members:

$$R'_\lambda = \sum_{k=1}^{N} f_k R_{k\lambda} + \varepsilon_\lambda. \quad (5)$$

Here, $R'_\lambda$ is the modeled mixture, $f_k$ represents the fractions of each of $k$ end members, $R_{k\lambda}$ is the reflectance

Fig. 3. Field examples of the stream bank morphologic scenarios evaluated in this study, from the Hollywood Meadow reach of Soda Butte Creek in Yellowstone National Park. Gradually sloping gravel bar in foreground and abrupt, vegetated cutbank on opposite side of channel. Photo courtesy of Dr. Andrew Marcus.

spectrum of the $k$th end member, and $\varepsilon_\lambda$ is a wavelength-specific error term; a unit sum constraint is typically imposed on the $f_k$ as well (Roberts et al., 1998). For our analysis of stream bank mixtures, we use Gaussian elimination to determine the least-squares optimal two-end member model for each bank scenario. One end member is the bank material reflectance spectrum and a single Hydrolight-modeled spectrum serves as the aquatic end member. For the gravel bar scenario, we evaluated the sensitivity of the mixture model to aquatic end member selection by computing bank fractions using three different water spectra: 1) the Hydrolight spectrum for the mean depth along the submerged portion of the bank slope, typically 5–10 cm depending on $f_b$ and $\theta_b$; 2) a fixed water spectrum of moderate depth, as might be obtained by selecting an image end member from the channel talweg; and 3) the spectrum for the greatest depth in the Hydrolight database, 1.5 m. For the vegetated cutbank, the water end member was taken as the Hydrolight spectrum corresponding to the depth of the channel bed $z_b$. To assess the feasibility of unmixing stream bank spectra, we compared the modeled bank fractions to the input $f_b$ used to parameterize each simulated bank scenario.

## 3. Results

### 3.1. Effects of sun–streambed geometry on upwelling spectral radiance

In topographically complex, meandering stream channels, the solar irradiance incident upon the channel bed will vary spatially as a function of solar geometry and local streambed slope and aspect. Fig. 4 illustrates the effect of solar–streambed geometry, expressed as the percent difference in $L_{u,690}$ relative to a flat bed, for a range of in-air solar zenith angles $\theta_s$, slope aspects $\varphi$ (defined as the angular difference between the solar azimuth and slope direction), and bed slopes $\theta_b$. For low $\theta_s$ and low to moderate $\theta_b$, topographic effects are minimal for small $\varphi$ (i.e., sun shining directly onto the slope) but become substantial for larger $\varphi$, with the greatest modification of the solar beam's angle of incidence onto the streambed occurring at $\varphi$=180° when the bed slopes down away from the sun (Mobley & Sundman, 2003). As $\theta_s$ increases to 40° or 50°, $L_u$ can be increased by nearly 20% relative to a flat bottom when a moderately steep bed slope faces the sun or reduced by up to 100% when the aspect is less favorable. For a fixed solar geometry (i.e., time of data collection), topographic effects

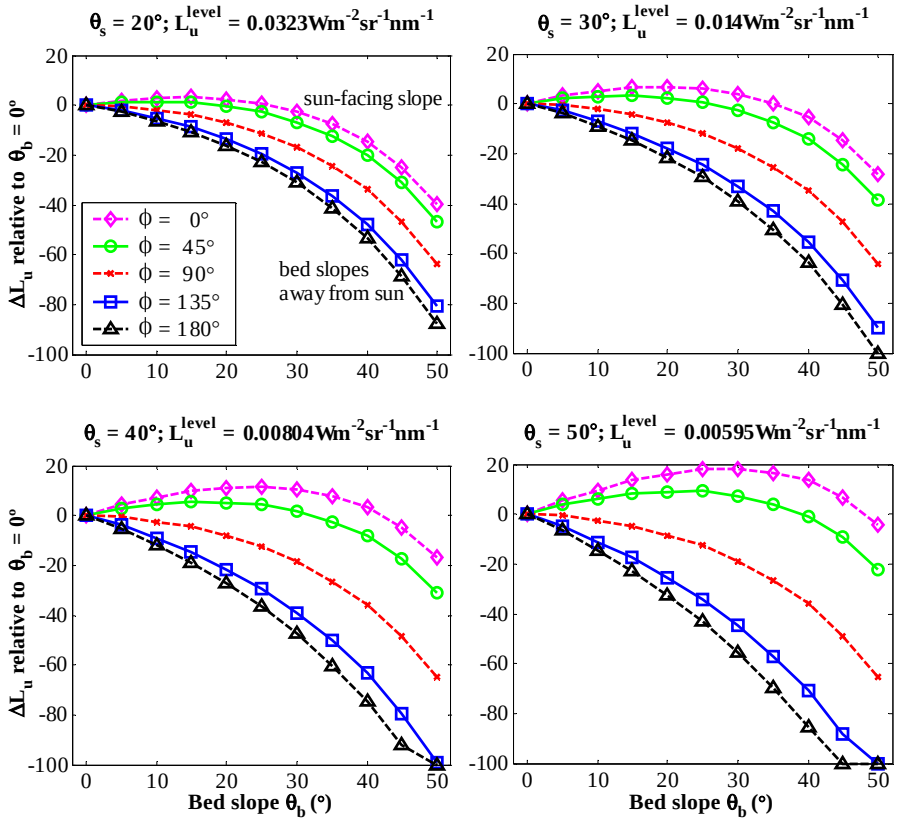


Fig. 4. Effect of solar geometry and streambed slope $\theta_b$ and aspect $\varphi$ on the upwelling spectral radiance $L_u$ (at 690 nm) from a shallow stream channel. Each panel represents a different solar zenith angle $\theta_s$ (in air) and lines represent different aspects $\varphi$, defined as the angular difference between the solar azimuth and the slope direction. The streambed faces the sun for small $\varphi$ and slopes down away from the sun for large $\varphi$. Changes in radiance $\Delta L_u$ are expressed as percentages of the equivalent level bottom $L_u$. Depth is 0.3 m and substrate is periphyton.

are clearly more pronounced for steeper bed slopes, such as those along channel banks. Although bed slopes of 50° might not be common in alluvial rivers, especially those with non-cohesive banks, even for a more typical pool exit slope of 10° (e.g., Thompson & Hoffman, 2001) and a fixed $\theta_s$, differences in $\varphi$ alone could still create a 10–15% range in $L_u$.

### 3.2. Effects of sub-pixel variability in depth

For smaller or more complex channels and/or coarser sensor spatial resolutions, many, if not most, image pixels will encompass relatively fine-scale morphologic features and thus a range of depths. For the hypothetical stepped streambed in Fig. 2b, the *REDUB* exhibited spectrally-dependent residuals which varied with $f_{deep}$ and step height $z_{deep}-z_{shallow}$ (Fig. 5). For a moderate step height of 20 cm, the *REDUB* matched the area-weighted mean depth (thin, dashed lines in Fig. 5) at shorter, blue wavelengths but in the red portion of the spectrum positive *REDUB* residuals, defined as the difference between the area-weighted mean depth and the *REDUB*, indicated that depth was underestimated. The magnitudes of these residuals were least (1 cm) when $f_{deep}$ was either large (0.9) or small (0.1) and greatest when the pixel contained equal amounts of deep and shallow water, up to 3 cm in the near-infrared for $0.4 \leq f_{deep} \leq 0.6$. The gaps in the *REDUB* spectra plotted in Fig. 5 correspond to a crossover region of equal $L_u$ for all depths, with scattering by suspended sediment dominant at shorter wavelengths and absorption by pure water prevalent in the red and near-infrared (Legleiter et al., 2004). As the step height increased to 40 or 60 cm, the *REDUB* residuals became increasingly positive, indicating larger underestimates of the area-weighted mean depth. For the 60 cm step, the *REDUB* bias reached 22 cm in the NIR for $f_{deep}$=0.7 and was 5 cm even in the visible at 675 nm. For smaller $f_{deep}$ (i.e., shallower area-weighted mean depths), the *REDUB* residuals were smaller but can still be on the order of 8 cm for high steps. This effect was also modulated by the substrate, and the high NIR reflectance of periphyton also could have contributed to the large *REDUB* residuals in Fig. 5; the magnitude of these residuals might be reduced for other substrates with lower NIR reflectance. In general, for pixels with both a range of depths and a non-homogeneous substrate, the pixel-scale $L_u$ will depend on the spatial distribution of benthic cover types relative to the bed topography, as well as the scattering properties of the water column. In any case, our simulations indicated that the juxtaposition of deep and shallow water within a single pixel caused spectrally-based depth retrieval to underestimate the true mean depth because the shallow water made an areally disproportionate contribution to the aggregate, pixel-scale radiance, effectively drowning out the radiance contributed from the deeper water portion of the pixel.

We also performed a second, somewhat more realistic set of simulations based upon beta distributions of depth within an image pixel. By varying the $\alpha$ and $\beta$ parameters of the

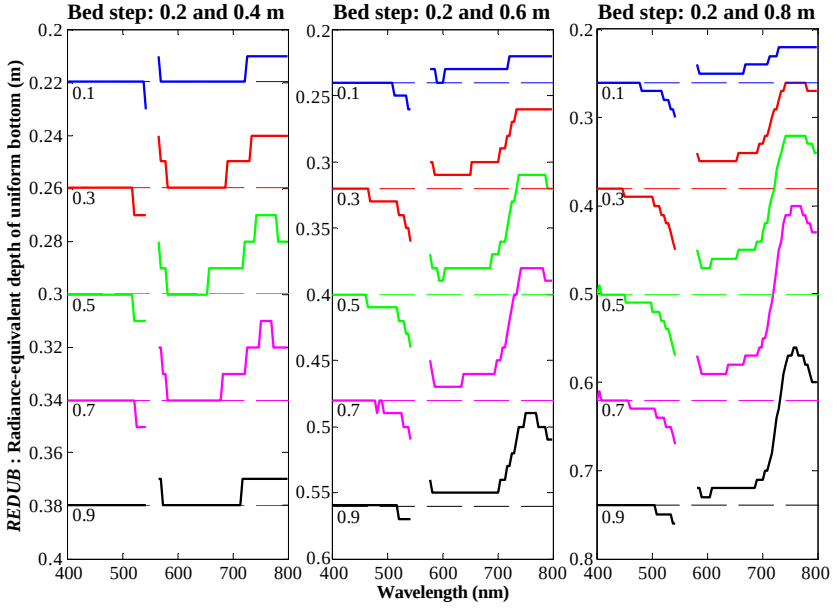


Fig. 5. *REDUB* spectra for simulated stepped streambeds of various step heights ($z_{deep}-z_{shallow}$) and fractions of deep water $f_{deep}$ (labeled for each line). The radiance-equivalent depth of a uniform bottom (*REDUB*) is defined at each wavelength as the depth of a uniform bottom at which the modeled Hydrolight $L_u$ spectrum is closest in absolute value to the $L_u$ for the mixed, variable depth pixel. The thin dashed lines in each panel represent the area-weighted mean depth for the specified $f_{deep}$ and the *REDUB* residual is defined as the difference between this true depth and the *REDUB* at each wavelength. The gap in each *REDUB* spectrum represents a region of equal radiance for all depths (see text for explanation). Substrate is periphyton and solar zenith angle $\theta_s$ is 30° (in air). (For interpretation of the references to color in this figure legend, the reader is referred to the web version of this article.)

beta pdf (Eq. (4)), we created depth distributions representative of sloping bottoms (uniform pdf; Fig. 6a), relatively flat bottoms (strongly peaked, symmetric distribution; Fig. 6d), and streambed configurations featuring either predominantly shallow (Fig. 6e) or predominantly deep (Fig. 6f) water. The performance of a ratio-based depth retrieval algorithm in the presence of such sub-pixel depth variability was evaluated in terms of the *REDUB* ratio, the depth of a uniform bottom for which the ln ($L_{u,560}/L_{u,690}$) ratio is equivalent to that computed for the simulated pixel. The *REDUB* ratio consistently reproduced the area-weighted mean depth of the pixel, even for negatively skewed depth distributions (Fig. 6f, h), unlike the spectrally-dependent residuals observed when the *REDUB* was retrieved from the Hydrolight database on a band-by-band basis.

### 3.3. Effects of sub-pixel variability in bottom albedo

Because $L_u$ is sensitive to both depth and bottom albedo, sub-pixel substrate heterogeneity could influence spectrally-based depth estimates even when depth is uniform at the pixel scale. Reflectance spectra for pure limestone and periphyton substrates are plotted in Fig. 7a and the panels below contain *REDUB* spectra (lines) and *REDUB* ratio depth estimates (points) for mixtures of these two substrate end members at depths of 30 and 60 cm (indicated by the dashed line in each panel). Fig. 7b and d illustrate the results of simulating $L_u$ for a mixed substrate comprised of both periphyton (covering a fraction $f_p$ of the substrate) and limestone (covering the remaining $1-f_p$), but then restricting the search of the Hydrolight database to consider only the pure periphyton end member when retrieving the *REDUB* for the mixed pixel. Similarly, $L_u$ spectra for these periphyton/limestone mixtures were compared to the pure limestone end members in the Hydrolight database to obtain the *REDUB* spectra and *REDUB* ratio values shown in Fig. 7c and e; *REDUB* retrievals were limited to depths less than 1 m in all cases. In essence, this analysis quantifies the depth retrieval error that would be incurred if substrate heterogeneity were

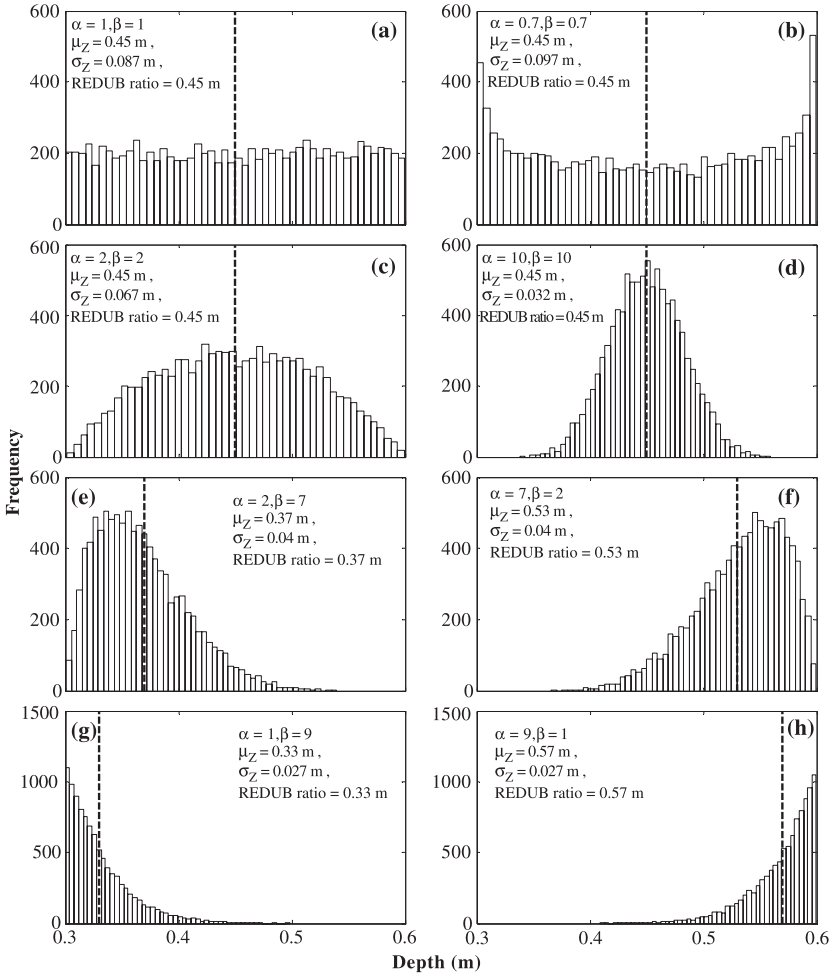


Fig. 6. Effects of sub-pixel bottom topography, simulated using beta distributions, on ratio-based depth retrieval. The dashed lines in each panel correspond to the *REDUB* ratio, defined as the depth of a uniform bottom for which the ln ($L_{u,560}/L_{u,690}$) ratio calculated for a Hydrolight spectrum is equivalent to that computed for the simulated, variable-depth pixel. Each panel also lists the parameters ($\alpha$ and $\beta$) used to generate the depth distribution, the area-weighted mean depth $\mu_z$, and the standard deviation of depth $\sigma_z$. Substrate is periphyton and $\theta_s$=30° (in air).

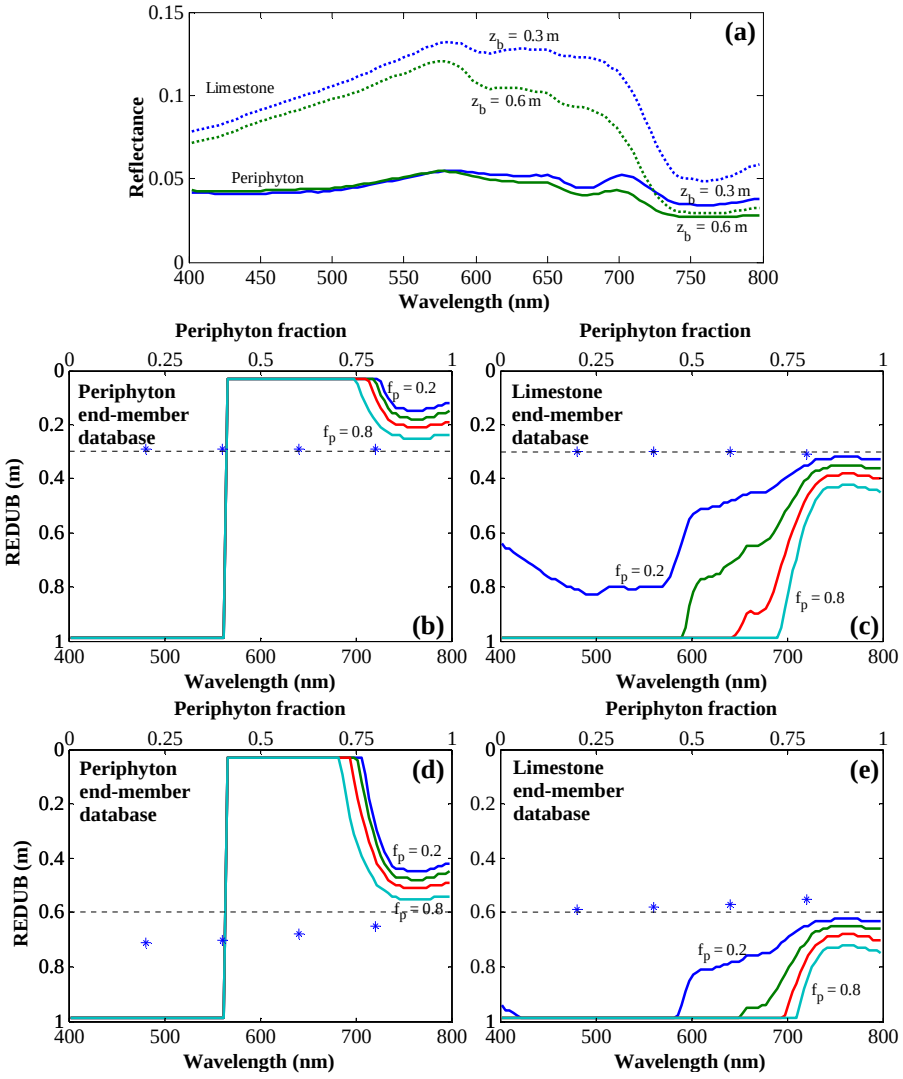


Fig. 7. Effects of fine-scale substrate heterogeneity on spectrally-based depth estimates. (a) Hydrolight-modeled reflectance spectra for limestone and periphyton substrates at depths of 30 and 60 cm. (b–d) *REDUB* spectra (lines, referring to bottom axis, with the periphyton fraction $f_p$ for each line labeled on the plot) and *REDUB* ratio values (points, referring to top $x$-axis) for various periphyton fractions, using both pure periphyton (b and d) and pure limestone spectra (c and e) from the Hydrolight database as references for comparison with the simulated limestone/periphyton mixtures. Bottom is level at the depth indicated by the dashed line in each panel and $\theta_s$ is fixed at 30° (in air). (For interpretation of the references to color in this figure legend, the reader is referred to the web version of this article.)

neglected and a single benthic end member was used throughout an image.

When comparing the simulated constant depth/mixed substrate $L_u$ spectra to the pure periphyton database, the *REDUB* "saturated" and was assigned the greatest depth in the database at wavelengths up to 560 nm, irrespective of the actual bottom depth or $f_p$ of the simulated mixture. At this end of the spectrum, an increase in $z_b$ corresponded to an increase in $L_u$ due to scattering by suspended sediment, and the increased pixel-scale $L_u$ due to the presence of bright limestone had the same effect as an increase in volume reflectance and effectively caused the pixel to appear deeper than if the substrate were composed of pure periphyton. Conversely, in the red portion of the spectrum $L_u$ and $z_b$ were inversely related and the *REDUB* for the mixed pixel was the minimum depth in the database because the increased $L_u$ associated with the limestone substrate caused the pixel to appear shallower than a streambed completely covered by periphyton. Only in the NIR were differences in $f_p$ expressed in the *REDUB*, with higher $f_p$ corresponding to greater *REDUB* as the radiance contribution from the limestone portion of the pixel was reduced, although the *REDUB* consistently underestimated the actual depth. This convergence in the NIR could be due to the more similar reflectance of the limestone and periphyton substrates at these wavelengths and/or due to stronger absorption by the water itself, which subdues the effect of bottom albedo on $L_u$.

An opposite pattern was observed when the pure limestone substrate end member was used as the reference for *REDUB* retrievals from the simulated periphyton/limestone mixtures. In this case, *REDUB* spectra were more sensitive

to $f_p$ but still tended to saturate and take on the value of the deepest depth within the database for wavelengths extending throughout the red portion of the spectrum for high $f_p$. The lower bottom albedo of the periphyton substrate reduced $L_u$ for the mixed pixel and therefore caused the bottom to appear deeper than would a periphyton-free limestone substrate, and at an actual depth of 30 cm, *REDUB* overestimated $z_b$ by up to 50 cm in the green region of the spectrum even when $f_p$ was only 0.2. The crossover at 560 nm was absent when pure limestone was used as a reference because, unlike the darker periphyton, the reflectance of the limestone substrate exceeded the scattering-induced volume reflectance of the water column, illustrating the importance of bottom contrast for depth retrieval. The *REDUB* also overestimated the true depth throughout the red and NIR and only at wavelengths of 720 nm or greater, where transmittance through the water column was reduced and the reflectance difference between limestone and periphyton less pronounced, did the *REDUB* begin to converge on the true depth. These results indicate that two different estimates of depth would be retrieved, depending on which pure substrate served as a reference: depth would be overestimated at all wavelengths if limestone were assumed and would be either over- (short wavelengths) or underestimated (long wavelengths) if a periphyton-coated streambed was assumed instead.

In contrast to the sensitivity of the wavelength-specific *REDUB* spectra to mixed substrates, the *REDUB* ratio was much more robust to sub-pixel substrate heterogeneity (points in Fig. 7b–e, referring to the top *x*-axis of each panel). For an actual depth of 30 cm, the *REDUB* ratio consistently reproduced the actual $z_b$ regardless of whether the periphyton or limestone database was used as a reference. For mixed substrates at a depth of 60 cm, the *REDUB* ratio retrieved from the periphyton database overestimated $z_b$ by up to 10 cm for small $f_p$ but agreement improved for larger $f_p$. When the limestone database served as the reference, the *REDUB* ratio reproduced $z_b$ for small $f_p$ and underestimated $z_b$ by only 3 cm for large $f_p$.

### 3.4. Stream bank spectral mixture analysis

Fig. 8a and b illustrate the simple geometric representations of gravel bars and vegetated cutbanks used to simulate mixed streamside pixels as weighted linear combinations of the pure spectra for each bank material and the submerged channel bed. For the vegetated cutbank simulations, we used the Hydrolight spectrum corresponding to depth of the adjacent streambed as the aquatic end member. For the gravel bar mixture models, we considered spectra for three depths: 1) the mean depth along the bed slope off of the bar, which thus varied depending on $\theta_b$ and $f_b$; 2) a fixed, moderate depth ($z_b$=0.2 or 0.4 m); and 3) 1.5 m, the greatest depth in the Hydrolight database (a hypothetical infinitely deep-water column produced nearly identical results). The actual (simulated) and modeled bank fractions $f_b$ for four morphologic scenarios, computed using linear, unit sum-constrained two-end member models are plotted in panels c–f. Fig. 8c and e indicate that for gravel bars the modeled bank fraction is accurate to within a few percent for large $f_b$ but is consistently underestimated for water-dominated pixels. The magnitude of this error increases as $f_b$ decreases, with negative modeled bank fractions for the smallest actual $f_b$. Fraction errors were smaller, however, when a moderate fixed depth end member was used rather than the mean depth along the slope; using a deep-water spectrum further reduced the fraction error. These results imply that shallow-water spectra along gradually sloping bars tend to be very similar to exposed, possibly moist, gravel, and that more accurate unmixing of stream bank pixels could be achieved by selecting or modeling a deep-water end member with greater spectral contrast.

Although the radiance contribution from the exposed portion of a mixed pixel might be expected to overwhelm the submerged area and lead to overestimated, possibly super-positive bank fractions, $f_b$ was underestimated for our simulated mixtures and became negative at low $f_b$, even when a deep-water end member was used. We attribute this counterintuitive result to the use of relatively bright, dry gravel as a terrestrial end member but dark, wet gravel to define the bottom albedo for the water spectra (Fig. 1). This low reflectance substrate was actually darker than deep, open water due to volume scattering within the water column. Mixed pixels comprised primarily of water were therefore brighter than shallow water end members bearing the imprint of the dark gravel substrate, which dictated that the bright terrestrial end member would require a negative fraction in order to make the modeled mixture dark enough while still honoring the unit sum constraint. This effect was most pronounced for the smallest actual $f_b$ and steepest bar slopes, which contained the most (and deepest) water and were thus brightest at the pixel scale. The extreme case is illustrated in Fig. 8g, where a pixel containing only 10% gravel bar was unmixed using a shallow water end member that was actually brighter than the pixel-scale mixture, resulting in a large negative modeled $f_b$ and a 25% fraction error. Had a brighter substrate (i.e., limestone) been used to define the bottom albedo, the shallow water end members would have been brighter than open water, resulting in overestimated bank fractions. The choice of a terrestrial end member could also play a role, with bright spectra from high, dry bar tops producing different results, typically underestimated bank fractions, than darker spectra from lower on the bar surface, where wet sand might also be present. These results indicate that linear spectral unmixing of gravel bars is highly sensitive to end member selection and thus subject to considerable uncertainty.

For vegetated cutbanks, typically found opposite gravel point bars along the outside of meander bends, linear spectral unmixing of stream bank pixels appears much more promising. For actual bank fractions ranging from 0.1 to 0.9 and bed depths of 20 and 40 cm, the modeled $f_b$ reproduce

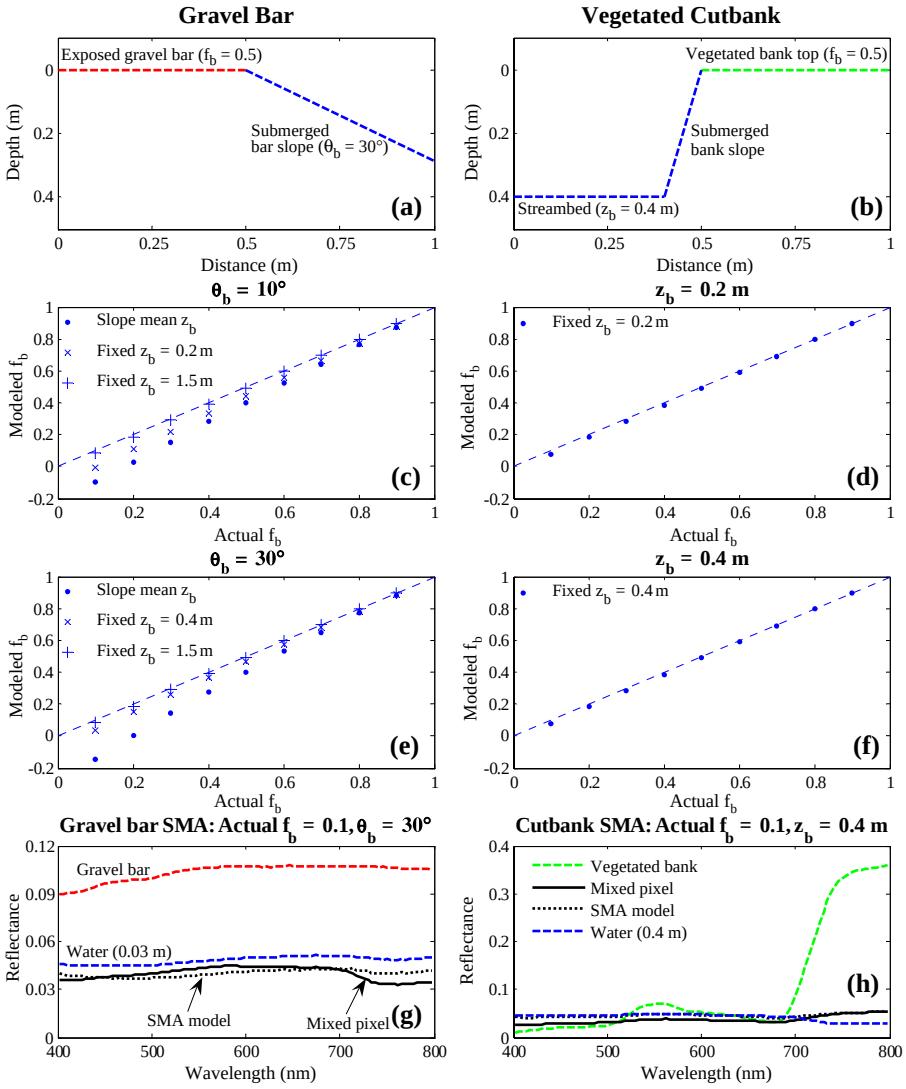


Fig. 8. Spectral characteristics of mixed terrestrial/aquatic pixels along stream banks. Geometric configuration of simulated gravel bars (a) and vegetated cutbanks (b), with plots of the actual and modeled bank fractions $f_b$ for each morphologic scenario and end member pair shown in panels (c–f); dashed lines represent the 1:1 line where the modeled $f_b$ reproduces the actual $f_b$ for the simulation. Panels (g) and (h) illustrate the end member spectra, simulated mixed pixels, and SMA-modeled mixtures for the case of small $f_b$.

the fractions used to simulate the mixtures almost exactly, even for the small actual bank fractions that proved most problematic for gravel bars (Fig. 8h). Unlike gravel bars with reflectance spectra similar to the adjacent substrate, vegetation along the banks is quite spectrally distinct from aquatic end members, particularly in the near-infrared. This enhanced spectral contrast allows for accurate solution of the mixing model and also reduces the sensitivity of the resulting fractions to end member selection.

### 3.5. Application to the Lamar River AISA scene

The simulations described in the preceding sections were motivated by our field experience in the Lamar River Basin and by the need to establish a physically-based theoretical foundation for analyzing archival image data for which field measurements were unavailable. As an example of the importance and applicability of our simulation-based results, we developed a ratio-based relative depth map and two-end member spectral mixture models from an AISA hyperspectral image of the Lamar River (Fig. 9a). A relative depth value was assigned to each in-stream pixel by 1) computing the natural logarithm of the ratio of apparent reflectances (Section 2.1) measured in spectral bands centered at 555 and 693 nm to obtain a variable linearly related to water depth; 2) subtracting the minimum ratio value from every pixel, in effect setting the minimum depth to zero; and 3) dividing each pixel by the mean of all in-stream pixels. The resulting image (Fig. 9b) highlighted a shallow gravel bar on the left side of the channel and a narrow talweg along the outer bank, illustrating the complex, fine-scale morphology typical of this dynamic fluvial system. The relatively coarse image data dictated that this filtered, 2.5 m representation of the true bed topography would include a large proportion of

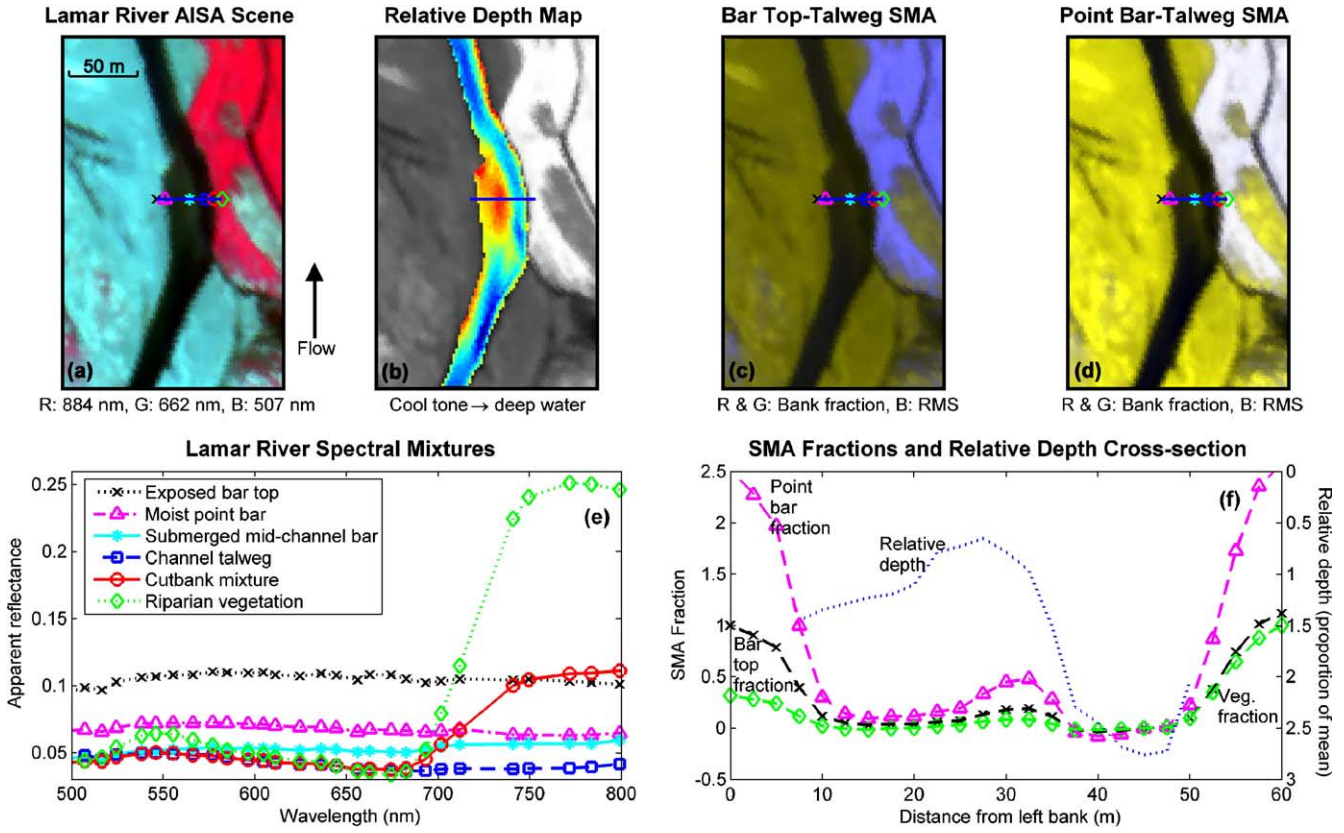


Fig. 9. (a) AISA hyperspectral image of the Lamar River; (b) relative depth map with cooler tones indicating deeper water (background is the 884 nm band); (c) stream bank mixture models for the exposed bar top and (d) moist point bar end members; (e) apparent reflectance spectra extracted along the transect shown with the blue line in (a–d); and (f) modeled fractions (left axis) and relative depth cross-section (right axis).

variable depth pixels analogous to our simulations. These morphologic scenarios provided theoretical evidence that the log-transformed band ratio provides an unbiased estimate of the pixel-scale mean depth, although replacing point measurements of depth with an area-weighted average will inevitably entail a loss of information (i.e., reduction in variance). The simulations thus justified our interpretation of image-derived depth maps while also informing us of their limitations and inherent uncertainties.

Similarly, two-end member spectral mixture models of the Lamar River were consistent with the results obtained for simulated stream bank mixtures (Section 3.4). We created models that unmixed the wetted channel from 1) the exposed, presumably dry bar top; 2) the point bar immediately adjacent to the channel, which was probably somewhat moist; and 3) riparian vegetation on top of the outside cutbank. A single water end member was selected from the talweg and a unit-sum constraint was included in all three models. As predicted by our simulations, the high spectral contrast between the channel and the vegetated cutbank ensured accurate unmixing on the right side of the river, as indicated by near-unity vegetation fractions (Fig. 9f) and low RMS errors (not shown). The two bar–channel mixture models are displayed as false-color composites in Fig. 9c and d, and, as expected, the gradually sloping left margin of the river proved more problematic. Although the two bar end members resulted in fraction images with similar spatial patterns, the bank fraction estimated using the dark point bar was consistently higher than when a brighter, bar top spectrum served as the terrestrial end member; this is expressed as a darker and/or greener tone in Fig. 9c relative to d, which has an identical contrast stretch. The darkness of the wetted channel in these images indicates very small, mostly negative, bank fractions and small RMS errors, suggesting that relatively deep water can be distinguished from either bar end member. For the shallow mid-channel bar, however, the slightly lighter, yellow tone indicates a larger bank fraction and suggests that water depth has a confounding effect on linear mixture models. On the opposite, densely vegetated bank, the blue hue in Fig. 9c represents large RMS errors when the brighter, bar top end member was used, while the white area of 9d indicates both large RMS errors and super-positive bank fractions for the darker, point bar end member. Both of these images suggest that simple two-end member models failed to provide a complete description of the riparian environment.

The image spectra in Fig. 9e confirmed that accurate unmixing of stream banks was favored by the large NIR reflectance difference between the channel and adjacent riparian vegetation and compromised by the similar spectral shapes for submerged and exposed portions of gravel bars, which appeared to differ only in overall brightness. The

difficulty of unmixing bar–channel mixtures could be due to both a lack of spectral contrast and the "visibility" of the terrestrial end member through shallow water, resulting in considerable spectral confusion. This hypothesis was supported by the cross-sections of relative depth and end member fractions in Fig. 9f, where the bar fractions for both end members mimic the channel geometry, notably the mid-channel bar, revealed by the log-transformed band ratio, with a gradual transition to high bar fractions along the left bank.

## 4. Discussion

### 4.1. Limitations and applicability

The first-order analysis presented in this study provided an indication of the likely effects of sub-pixel variability of depth and/or bottom albedo and stream bank spectral mixtures upon image-derived depth estimates, but our approach was limited in several important respects. First, our representation of the water column optical properties was simplistic and could be refined by incorporating chlorophyll, dissolved organic matter, and vertical concentration gradients; in situ measurements of absorption and scattering coefficients would be invaluable. Second, our simulated pixels did not incorporate sensor spectral response or point spread function and assumed linear mixing, ignoring in-water adjacency affects. We also did not consider the case where both depth and substrate vary simultaneously on a sub-pixel scale. Sensor characteristics could be included with appropriate technical data, but the problems of intimate mixtures and co-varying depth and bottom albedo present greater challenges. Finally, our simulations were based on only a handful of measured spectra from one small stream in Yellowstone National Park and these bank material and substrate end members might not be representative of other rivers in different environments. Nevertheless, we believe that the analysis presented here is sufficiently general to illustrate, in a physically-based manner, important relationships among channel morphology, sensor spatial resolution, and the uncertainty inherent to spectrally-based depth retrieval.

### 4.2. Advantages of ratio-based depth retrieval

The results outlined above demonstrated the utility of the log-transformed band ratio for estimating water depth and indicated that the technique is particularly well-suited to complex fluvial environments like the Lamar River. A primary advantage of the ratio-based algorithm is that the site-specific normalization inherent to the ratio implicitly accounts for solar geometry and specular reflection from the water surface. Because this surface reflectance is spectrally flat (Legleiter et al., 2004), it will affect both bands equally and cancel during the ratio calculation. Unlike oceanographic applications where sun glint can be attributed primarily to wind-induced waves and corrected uniformly across an image, pixel-by-pixel removal of the specular component of the upwelling radiance is critical in rivers because the flow-related turbulence responsible for the irregularity of the water surface varies spatially as a function of depth, velocity, and substrate particle size.

Similarly, although the topographic effects described in Section 3.1 could severely compromise analyses based on the absolute magnitude of $L_u$, ratio-based depth retrieval algorithms should be less affected. Because the incidence angle terms in Eq. (2) are spectrally invariant and occur in both the numerator and denominator, bed topography will be implicitly accounted for in each individual pixel. The accuracy and precision of image-derived estimates will still be lower in areas with steep bed slopes and/or an unfavorable aspect because $E_d$ and thus $L_u$ will be reduced. When the bed is poorly illuminated, changes in depth will correspond to very small changes in $L_u$ that could be below the detection limit of many imaging systems (Legleiter et al., 2004). Because streambed slope and aspect are spatially variable, the magnitude of these topographic effects will also vary throughout an image to an extent that will not, in practice, be known a priori. Acquiring data at lower $\theta_s$ will reduce topographic effects but could introduce problems (i.e., sensor saturation) related to specular reflection from the water surface; Mobley (1999) cautions that sun glint is inevitable when both solar and view zenith angles are small. Collecting data at off-nadir views could mitigate this effect but might complicate flight planning and geometric correction.

Our simulations of beta-distributed depths and substrate patches also suggested that ratio-based depth retrieval is robust to fine-scale bottom morphology and substrate heterogeneity. Whereas the *REDUB* spectra calculated for stepped streambeds were subject to a strong, spectrally-dependent bias toward shallower water, the *REDUB* ratio consistently reproduced the area-weighted mean depth for uniform, symmetric, and highly skewed depth distributions. When bright limestone and dark periphyton substrates were combined in varying proportions at a fixed depth, the spectral *REDUB* was again strongly biased while the *REDUB* ratio reproduced the actual depth for shallow water and produced relatively small errors in deep water. The robustness of the band ratio in these simulations reflects the theoretical basis of the technique—whereas a change in substrate reflectance affects both ratio bands similarly, an increase in depth produces a much greater decrease in radiance in the band with stronger attenuation (Dierssen et al., 2003). Our results support the finding of Stumpf et al. (2003) that ratio values for different substrates at similar depths are similar to one another and imply that the ratio-based algorithm is more appropriate for complex in-stream habitats than alternative approaches that do not include such normalization. For example, the comparative spectral classification method of Louchard et al. (2003), which

assigns depth and substrate reflectance values to image pixels by selecting the Hydrolight-modeled spectrum most similar to the radiance measured by the imaging system, might not be able to account for spatial variations in specular reflectance and bottom slope and could also be sensitive to sub-pixel mixtures of depth and/or bottom albedo. Although this type of sophisticated spectrally-based analysis could prove useful in the future, at present the ratio-based algorithm provides a simple, effective method for mapping river channel morphology.

### 4.3. Problems and prospects for spectral mixture analysis

The simple, two-end member models for mixed pixels along stream banks described in Section 3.4 and applied to a hyperspectral image of the Lamar River in Section 3.5 indicated that the ability to unmix streamside spectra is strongly dependent on bank morphology. Specifically, whereas bank fractions for vegetated cutbanks were modeled very accurately, spectral mixture models developed for gravel bars typically featured relatively large fraction errors. The differences between these two bank types illustrated the importance of spectral contrast and demonstrated the difficulty of discriminating between a shallow, submerged gravel bed and an adjacent, exposed bar surface. Our analysis of the gravel bar scenario also indicated that $f_b$ estimates were sensitive to the selection of both terrestrial and aquatic end members, with smaller fraction errors for deep-water spectra and bank fraction overestimates associated with darker terrestrial spectra. These results clearly indicate that a greater degree of confidence can be assigned to mixture models developed for steep, vegetated banks than for gradually sloping gravel bars. This finding implies that spectral mixture analysis will be a more reliable tool for some channel morphologies, such as meandering meadow streams with cohesive banks, than for others, such as bedload-dominated braided channels with numerous gravel bars.

The sensitivity to both morphology and end member selection observed in our simulations implies that more sophisticated multiple end member spectral mixture analysis (MESMA), in which the end members used to model mixed spectra are allowed to vary on a pixel-by-pixel basis (Roberts et al., 1998), might be a more appropriate method for fluvial environments. By coupling bank and substrate spectra with a radiative transfer model such as Hydrolight, MESMA could also be useful for depth retrieval. Hedley and Mumby (2003) have proposed an SMA-based method of mapping depth and sub-pixel proportions of benthic end members, but their approach does not provide any measure of the error in the mixture model (e.g., root mean square error or spectral residuals; see Roberts et al., 1998) and has not yet been tested on real data. Future application of SMA to rivers will require the development of more extensive substrate spectral libraries and the acquisition of more advanced, hyperspectral image data, which should involve careful evaluation of the tradeoffs among spectral detail, spatial resolution, and radiometric precision.

### 4.4. Implications for remote measurement of river channel change

The fundamental motivation for this study was to determine whether remotely sensed data could be used to estimate water depth with sufficient accuracy and precision to document subtle changes in channel morphology. Our results indicate that this important question cannot be answered with broad generalizations but must instead be addressed on a case-by-case basis. The analysis of simple morphologic scenarios presented here illustrated how streambed slope and aspect, bed topography, and substrate heterogeneity influence the upwelling spectral radiance from a shallow stream channel. These simulations also suggested, however, that the simple, ratio-based depth retrieval algorithm is robust and well-suited for complex fluvial systems, consistently reproducing the area-weighted mean depth when depth and/or substrate vary on a sub-pixel scale. The ratio calculation also implicitly accounts for specular reflectance and topographic effects, but solar–streambed geometry could still adversely affect depth retrieval at high solar zenith angles and/or where the bed slopes away from the sun. In topographically complex meandering rivers, the resolution and reliability of depth estimates could thus vary from one pixel to the next.

In fact, the primary implication of our study is that the relationship between sensor spatial resolution and channel morphology establishes a set of complex, spatially variable controls on the accuracy and precision with which river channels can be remotely mapped. For example, both our simulations and the mixture models we derived from the Lamar River hyperspectral image indicate a strong morphologic dependence, with SMA-derived bank fractions estimated more accurately for steep, vegetated banks than for gravel bars. This effect is, of course, mediated by sensor spatial resolution because the proportion of mixed terrestrial/aquatic pixels will decrease as the ratio of channel width to image pixel size increases. For the fluvial geomorphologist, these results imply that sub-pixel refinement of width measurements (i.e., multiplying $f_b$ by the pixel size for the end-points of a cross-section) will likely be more accurate along the outer bank of a meander bend than along the opposite point bar. If this hypothesized pattern holds true, a greater degree of confidence can be assigned to lateral migration and pool scour along the outer bank than to point bar growth and bed aggradation on the inner bank. Within the channel proper, the ability to obtain realistic representations of pools, riffles, and other habitat features from digital image data will depend in a complex and spatially variable manner upon both the spatial resolution of the imaging system and the typical dimensions of channel features. If the spatial frequency of bed elevation change within the channel exceeds the sampling frequency of the

sensor, morphologic detail will be obscured, with the discrepancy between representation and reality becoming more pronounced as this frequency difference increases. In essence, the morphology of the channel complicates attempts to document that morphology using remote sensing techniques, and a spatial resolution that is adequate for one reach might not be appropriate for other, more complex channel segments.

Given this intimate linkage between sensor spatial resolution and channel morphology, the selection of an appropriate pixel size for specific studies becomes an important practical question. Because the log-transformed band ratio could provide an unbiased estimate of the area-weighted pixel-scale mean depth, the choice of a spatial resolution does not necessarily need to involve radiative transfer models or complicated hydrologic optics but can instead be posed in terms of sample design. Efficient use of remotely sensed data for river research and management will require familiarity with the channels of interest along with clear statements of the specific objectives of each study. We propose that although the accuracy and precision of image-derived depth estimates are complicated, spatially variable functions of channel morphology and sensor characteristics, they are nonetheless governed by fundamental physical processes which can be modeled to quantify the resolution and reliability of spectrally-based depth retrieval. Research toward this goal is needed to develop operational guidelines and define realistic expectations for remote sensing of rivers.

## 5. Conclusion

The contribution of remote sensing technology to river research depends on the ability to obtain from digital image data quantitative information on the channel characteristics of interest with the accuracy and precision required by specific applications. In this study, we evaluated the effects of sub-pixel variations in depth and bottom albedo on image-derived depth estimates and the role of morphology and end member selection in spectral mixture analysis of stream bank pixels. Using a radiative transfer model, we generated a database of spectra for various depths and substrate types, which we then coupled (assuming linear mixing) to various morphologic scenarios including a planar sloping streambed, a stepped bed, beta distributions of fine-scale depths, and heterogeneous substrates. These simulations indicated that although the upwelling spectral radiance from a shallow stream channel can be highly sensitive to each of these factors, simple, ratio-based depth retrieval algorithms are robust to topographic effects, fine-scale bottom morphology, and patchy substrates. For mixed pixels along channel margins, our results indicated that bank fractions derived from two-end member mixture models were highly accurate for vegetated cutbanks but less reliable for gravel bars. These theoretical results were tested by producing a relative depth map and calculating bank and water fractions from a hyperspectral image of the Lamar River. The primary conclusions of this study are that the utility of remotely sensed data for characterizing fluvial environments depends strongly on the relationship between sensor spatial resolution and channel morphology and that the accuracy and precision of image-derived depth estimates are spatially variable and cannot be categorically defined. The ability of the ratio-based depth retrieval to consistently reproduce the area-weighted, pixel-scale mean depth for our simulated morphologic scenarios was encouraging, however, and future research will focus on developing methods for selecting an appropriate pixel size for different types of channels. A related goal crucial for application-oriented users of digital image data is to provide physically-based, quantitative estimates of the uncertainty inherent to remote mapping of river channel morphology.

## Acknowledgement

Andrew Marcus provided the spectroradiometer and thought-provoking discussions out on the stream in Yellowstone National Park. Additional help in the field was provided by Mark Fonstad, Kyle Legleiter, Annie Toth, Sharolyn Anderson, Will Jensen, Lorin Groshong, and Lisa, Alexandra, Rebecca and Geoffrey Marcus. The Hydrolight model was developed by Curt Mobley of Sequoia Scientific, and Lydia Sundman provided valuable implementation advice. Rick Lawrence and Mike Zambon of Montana State University made the Lamar River AISA image available to us; these data were acquired through a grant from the Environmental Protection Agency. Bob Crabtree of the Yellowstone Ecological Center provided logistical support. Funding sources included fellowships from the American Society for Engineering Education, the National Science Foundation, and the American Society for Photogrammetry and Remote Sensing and grants from the Water Resources Specialty Group of the Association of American Geographers, the California Space Institute, and the Graduate Division at UC Santa Barbara. The thoughtful comments of two anonymous reviewers also resulted in an improved final paper.

## References

Adams, J. B., Smith, M. O., & Gillespie, A. R. (1993). Imaging spectroscopy: Interpretation based on spectral mixture analysis. In C. M. Pieters, & P. A. J. Englert (Eds.), *Remote geochemical analysis: Elemental and mineralogical composition* (pp. 145–166). Cambridge: Press Syndicate of University of Cambridge.

Andrefouet, S., Berkelmans, R., Odriozola, L., Done, T., Oliver, J., & Muller-Karger, F. (2002). Choosing the appropriate spatial resolution for monitoring coral bleaching events using remote sensing. *Coral Reefs*, *21*, 147–154.

Andrefouet, S., Kramer, P., Torres-Pulliza, D., Joyce, K. E., Hochberg, E. J., Garza-Perez, R., et al. (2003). Multi-site evaluation of IKONOS data for classification of tropical coral reef environments. *Remote Sensing of Environment*, *88*, 128–143.

Ashmore, P. E., & Church, M. (1998). Sediment transport and river morphology: A paradigm for study. In J. B. Bradley (Ed.), *Gravel-bed rivers in the environment* (pp. 115–140). Highlands Ranch, CO: Water Resources Publications.

Bryant, R. G., & Gilvear, D. J. (1999). Quantifying geomorphic and riparian land cover changes either side of a large flood event using airborne remote sensing: River Tay, Scotland. *Geomorphology*, *29*, 307–321.

Bukata, R. P., Jerome, J. H., Kondratyev, K. Y., & Pozdnyakov, D. V. (1995). *Optical Properties and Remote Sensing of Inland and Coastal Waters* (p. 362). Boca Raton, FL: CRC Press.

Cox, C., & Munk, W. (1954). The measurement of the roughness of the of the sea surface from photographs of the sun's glitter. *Journal of the Optical Society of America*, *44*, 838–850.

Cracknell, A. P. (1998). Synergy in remote sensing—What's in a pixel? *International Journal of Remote Sensing*, *19*, 2025–2047.

Devore, J. L. (2000). *Probability and Statistics for Engineering and the Sciences* (p. 775). Pacific Grove, CA: Duxbury.

Dierssen, H. M., Zimmerman, R. C., Leathers, R. A., Downes, T. V., & Davis, C. O. (2003). Ocean color remote sensing of seagrass and bathymetry in the Bahamas Banks by high-resolution airborne imagery. *Limnology and Oceanography*, *48*, 444–455.

Downs, P. W., & Kondolf, G. M. (2002). Post-project appraisals in adaptive management of river channel restoration. *Environmental Management*, *29*, 477–496.

Gaeuman, D. A., Schmidt, J. C., & Wilcock, P. R. (2003). Evaluation of in-channel gravel storage with morphology-based gravel budgets developed from planimetric data. *Journal of Geophysical Research-Earth Surface*, *108*, 6001.

Gregg, W. W., & Carder, K. (1990). A simple spectral solar irradiance model for cloudless maritime atmospheres. *Limnology and Oceanography*, *35*, 1657–1675.

Harrison, A. W., & Coombes, C. A. (1988). An opaque cloud cover model of sky short wavelength radiance. *Solar Energy*, *41*, 387–392.

Hedley, J. D., & Mumby, P. J. (2003). A remote sensing method for resolving depth and subpixel composition of aquatic benthos. *Limnology and Oceanography*, *48*, 480–488.

Hedley, J. D., Mumby, P. J., Joyce, K. E., & Phinn, S. R. (2004). Spectral unmixing of coral reef benthos under ideal conditions. *Coral Reefs*, *23*, 60–73.

Lane, S. N. (1998). The use of digital terrain modelling in the understanding of dynamic river channel systems. In J. H. Chandler (Ed.), *Landform monitoring, modelling and analysis* (pp. 311–342). New York: John Wiley and Sons.

Lane, S. N., Westaway, R. M., & Hicks, D. M. (2003). Estimation of erosion and deposition volumes in a large, gravel-bed, braided river using synoptic remote sensing. *Earth Surface Processes and Landforms*, *28*, 249–271.

Legleiter, C. J., & Goodchild, M. F. (2005). Alternative representations of in-stream habitat: Classification using remotely sensed data, hydraulic modeling, and fuzzy logic. *International Journal of Geographical Information*, *19*(1), 29–50.

Legleiter, C. J., Marcus, W. A., & Lawrence, R. (2002). Effects of sensor resolution on mapping in-stream habitats. *Photogrammetric Engineering and Remote Sensing*, *68*, 801–807.

Legleiter, C. J., Roberts, D. A., Marcus, W. A., & Fonstad, M. A. (2004). Passive optical remote sensing of river channel morphology and in-stream habitat: Physical basis and feasibility. *Remote Sensing of Environment*, *93*, 493–510.

Louchard, E. M., Leathers, R. A., Downes, T. V., Reid, R. P., Stephens, F. C., & Davis, C. O. (2003). Optical remote sensing of benthic habitats and bathymetry in coastal environments at Lee Stocking Island, Bahamas: A comparative spectral classification approach. *Limnology and Oceanography*, *48*, 511–521.

Lyon, J. G., Lunetta, R. S., & Williams, D. C. (1992). Airborne multispectral scanner data for evaluating bottom sediment types and water depths of the St. Mary's River, Michigan. *Photogrammetric Engineering and Remote Sensing*, *58*, 951–956.

Marcus, W. A., Legleiter, C. J., Aspinall, R. J., Boardman, J. W., & Crabtree, R. L. (2003). High spatial resolution hyperspectral mapping of in-stream habitats, depths, and woody debris in mountain streams. *Geomorphology*, *55*, 363–380.

Mertes, L. A. K. (2002). Remote sensing of riverine landscapes. *Freshwater Biology*, *47*, 799–816.

Mertes, L. A. K., Smith, M. O., & Adams, J. B. (1993). Estimating suspended sediment concentrations in surface waters of the Amazon River wetlands from Landsat images. *Remote Sensing of Environment*, *43*, 281–301.

Mobley, C. D. (1994). *Light and Water: Radiative Transfer in Natural Waters* (p. 592). San Diego: Academic Press.

Mobley, C. D. (1999). Estimation of the remote-sensing reflectance from above-surface measurements. *Applied Optics*, *38*, 7442–7455.

Mobley, C. D., & Sundman, L. K. (2001). *Hydrolight 4.2 User's Guide* (p. 88). Redmond, WA: Sequoia Scientific.

Mobley, C. D., & Sundman, L. K. (2003). Effects of optically shallow bottoms on upwelling radiances: Inhomogeneous and sloping bottoms. *Limnology and Oceanography*, *48*, 329–336.

Prostka, H. J., Ruppel, E. T., & Christiansen, R. J. (1975). *Geologic map of the Abiathar Peak Quadrangle, Yellowstone National Park, Wyoming*. U.S. Geological Survey Geological Quadrangle Map GQ-1244, scale 1:62:500.

Roberts, D. A., Gardner, M., Church, R., Ustin, S., Scheer, G., & Green, R. O. (1998). Mapping chaparral in the Santa Monica Mountains using multiple endmember spectral mixture models. *Remote Sensing of Environment*, *65*, 267–279.

Stumpf, R. P., Holderied, K., & Sinclair, M. (2003). Determination of water depth with high-resolution satellite imagery over variable bottom types. *Limnology and Oceanography*, *48*, 547–556.

Thompson, D. M., & Hoffman, K. S. (2001). Equilibrium pool dimensions and sediment-sorting patterns in coarse-grained, New England channels. *Geomorphology*, *38*, 301–316.

Whited, D., Stanford, J. A., & Kimball, J. S. (2002). Application of airborne multispectral digital imagery to quantify riverine habitats at different base flows. *River Research and Applications*, *18*, 583–594.

Winterbottom, S. J., & Gilvear, D. J. (1997). Quantification of channel bed morphology in gravel-bed rivers using airborne multispectral imagery and aerial photography. *Regulated Rivers: Research and Management*, *13*, 489–499.

Wright, A., Marcus, W. A., & Aspinall, R. (2000). Evaluation of multispectral, fine scale digital imagery as a tool for mapping stream morphology. *Geomorphology*, *33*, 107–120.

Zaneveld, J. R. V., & Boss, E. (2003). The influence of bottom morphology on reflectance: Theory and two-dimensional geometry model. *Limnology and Oceanography*, *48*, 374–379.